

# Learning to Learn Weight Generation via Trajectory Diffusion

Yunchuan Guan<sup>1,2</sup> Yu Liu<sup>2</sup> Ke Zhou<sup>2</sup> Zhiqi Shen<sup>1</sup> Serge Belongie<sup>3</sup> Jenq-Neng Hwang<sup>4</sup> Lei Li<sup>3,4</sup>

## Abstract

Diffusion-based algorithms have emerged as promising techniques for weight generation, particularly in scenarios like multi-task learning that require frequent weight updates. However, existing solutions suffer from limited cross-task transferability. In addition, they only utilize optimal weights as training samples, ignoring the value of other weights in the optimization process. To address these issues, we propose Lt-Di, which integrates the diffusion algorithm with meta-learning to generate weights for unseen tasks. Furthermore, we extend the vanilla diffusion algorithm into a trajectory diffusion algorithm to utilize other weights along the optimization trajectory. Trajectory diffusion decomposes the entire diffusion chain into multiple shorter ones, improving training and inference efficiency. We analyze the convergence properties of the weight generation paradigm and improve convergence efficiency without additional time overhead. Our experiments demonstrate Lt-Di’s higher accuracy while reducing computational overhead across various tasks, including zero-shot and few-shot learning, multi-domain generalization, and large-scale language model fine-tuning. Our code is released at <https://anonymous.4open.science/r/Lt-Di-0E51>.

## 1. Introduction

Diffusion-based generative models have emerged as a breakthrough AI technology, achieving state-of-the-art performance in scenarios like audio, image, and video generation (Gozalo-Brizuela & Garrido-Merchán, 2023). Recent advancements in diffusion models for high-dimensional data generation have introduced a novel application domain: the generation of neural network weights. This technology avoids the overhead associated with gradient-based training

<sup>1</sup>Nanyang Technological University <sup>2</sup>Huazhong University of Science and Technology <sup>3</sup>University of Copenhagen <sup>4</sup>University of Washington. Correspondence to: Zhiqi Shen <zqshen@ntu.edu.sg>, Lei li <lilei@di.ku.dk>.

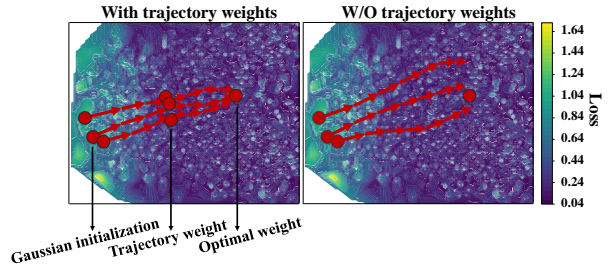


Figure 1. Inference chain of models trained with and without trajectory weights. In the 2D PAC reduced weight landscape, darker areas indicate lower downstream task loss. With the same initial points, trajectory weights help constrain the inference chain, whereas the diffusion chain of vanilla diffusion without trajectory weights tends to deviate from the optimal weights.

or fine-tuning, offering promising solutions for few-shot, multi-task, and multi-domain problems that require frequent weight updates.

Previous researchers leverage models such as Variational Autoencoder (VAE) (Kingma & Welling, 2014) and Hypernetwork (Ha et al., 2017) to learn the latent distribution of optimal weights for target tasks. OCD (Lutati & Wolf, 2023) and Meta-Diff (Zhang et al., 2024) attempt to use the diffusion model to simulate the weight optimization process. However, these approaches are constrained by single-level optimization frameworks and demonstrate limited capability for knowledge transfer between tasks, which subsequently impacts their generalization capacity for new tasks.

More importantly, current weight generation methods only utilize the optimal weights as training samples, overlooking the value of other weights along the optimization trajectory<sup>1</sup>. This limited utilization of available training resources results in suboptimal performance in terms of both accuracy and efficiency.

In this paper, (1) we propose to Learn to Learn Weight Generation via Trajectory Diffusion, i.e., Lt-Di. This method utilizes diffusion models within the framework of bi-level optimization. Benefiting from the generalization capability offered by bi-level optimization (i.e., learn to learn), Lt-Di

<sup>1</sup>We will denote such weight as trajectory weight in the following section for brevity.

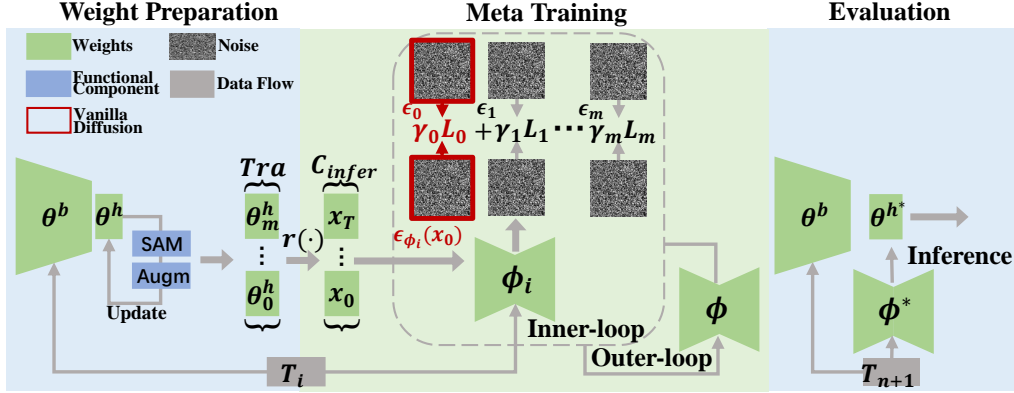


Figure 2. Workflow of Lt-Di. In the weights preparation stage, it updates  $\theta^h$  and constructs the optimization trajectory  $Tra_i = \{\theta_m^h, \dots, \theta_0^h\}$  for each task  $T_i$ . In the meta-training stage, it uses  $r(\cdot)$  to map optimization trajectory to the inference chain  $C_{infer} = \{x_T, \dots, x_0\}$  for diffusion learning. In the inner-loop of meta-learning, it performs trajectory diffusion and decouples functional components into the weight preparation stage for efficiency. In the evaluation stage, it uses the well-trained denoise  $\phi^*$  to generate optimal weights  $\theta^{h^*}$  for unseen task  $T_{n+1}$  without gradient computation. The red rectangle shows that trajectory diffusion is an extended version of vanilla diffusion with more observed data and loss functions.

enables fast weight generation across multiple tasks or domains. Figure 2 shows Lt-Di’s workflow, which consists of weight preparation, meta-training, and evaluation stages. (2) We extend the vanilla diffusion algorithm to trajectory diffusion, which leverages the weights along the optimization trajectory for training. As shown in Figure 1, when trained with trajectory weights, Lt-Di’s inference chain converges midway, making the final generated weights closer to the optimal weights. The above characteristics enable Lt-Di to achieve higher generation accuracy while tolerating fewer diffusion steps. (3) We analyze the convergence properties of the weight generation paradigm and introduce improvements. We decouple functional components, i.e., data augmentation (Hospedales et al., 2021) for robustness and sharpness-aware minimization (Foret et al., 2022) for convergence efficiency from the meta-training stage to the weight preparation stage, improving performance without additional time overhead.

Our contributions can be summarized as follows:

- We propose Trajectory Diffusion, which leverages a whole trajectory to guide the diffusion model’s inference chain.
- We propose Lt-Di, which combines meta-learning and trajectory diffusion to efficiently generate weights for unseen tasks.
- We analyze the convergency property of the weight generation paradigm and improve convergence efficiency without additional time overhead.

---

### Algorithm 1 Weight Preparation

---

**Require:** Model weights  $\theta = \{\theta^h, \theta^b\}$ , downstream loss function  $L_d(\theta)$ , perturbation magnitude  $\rho$ , and learning rate  $\alpha$ .

- 1: **for** each training step **do**
  - 2:   Add noised and rotated data (i.e., data augmentation)
  - 3:    $\epsilon \leftarrow \rho \frac{\nabla L(\theta)}{\|\nabla L(\theta)\|}$
  - 4:    $g_{\text{worst}} \leftarrow \nabla_{\theta^h} L(\theta + \epsilon)$  (i.e., SAM)
  - 5:    $\theta^h \leftarrow \theta^h - \alpha \cdot g_{\text{worst}}$
  - 6:   Record  $\theta^h$
  - 7: **end for**
  - 8: Select  $\theta^h$  and construct  $Tra = \{\theta_m^h, \dots, \theta_0^h\}$
  - 9: **Return**  $Tra$
- 

## 2. Methodology

In this section, we introduce Lt-Di’s workflow and provide a preliminary in Appendix C. The workflow of Lt-Di is shown in Figure 2, which consists of three stages: weight preparation, meta-training, and evaluation.

### 2.1. Weight Preparation

During the weight preparation stage, we collect weights and construct an optimization trajectory  $Tra_i$  corresponding to each task  $T_i$ . In alignment with research demonstrating the significant influence of final layers in fine-tuning (Raghu et al., 2020; 2017), and to optimize computational efficiency, we focus our attention specifically on the downstream network head  $\theta^h$  while maintaining the body  $\theta^b$  freezing. Specifically, we use  $T_i$  in the training set to up-

date  $\theta_h$  and record the corresponding optimization trajectory  $Tra_i = \{\theta_m^h, \dots, \theta_0^h\}$ . Note that  $\theta_m^h$  is Gaussian-initialized weight and  $\theta_0^h$  denotes the last weight recorded in the updating process<sup>2</sup>. Considering storage overhead and the complexity of the optimization problem, we don't collect all weights generated in each epoch. We detail the number of trajectory weight in Section 3.2.1.

Benefiting from such an indirect learning approach, we can advance functional components from inner-loop to the weight preparation stage. As shown in Figure 2, we add Sharpness Aware Minimization (SAM) for convergence efficiency and data augmentation for robustness. Meanwhile, the meta-training phase can start synchronously once a few weights are collected. Therefore, adding functional components during weight preparation doesn't incur additional time overhead. The specific process of weight generation stage is detailed in Algorithm 1.

## 2.2. Meta-Training.

In the meta-learning stage, we use REPTILE (Nichol et al., 2018) as the framework to ensure efficiency. Our meta-objective is defined specifically as learning a diffusion model  $\epsilon_\phi$  (i.e., denoiser) that can recover the Gaussian-initialized weights to the optimal weight  $\theta^{h^*}$  for the unseen task  $T_{n+1}$ . We employ the same U-Net denoiser architecture given by Rombach et al. (2022), and maintain this setup across all experiments in this paper. To learn on multiple tasks and enhance meta-learning, the denoiser needs additional condition states represented by the task embedding  $Emb_{T_i} = \theta^b(T_i)$ <sup>3</sup>. Considering empirical optimal weight  $\theta_0^h$  as the diffusion target  $x_0$ , we follow the setup of vanilla diffusion algorithm Denoising Diffusion Probabilistic Model (DDPM) (Ho et al., 2020). One of an inner-loop loss  $L_0$  can be written as:

$$L_0 = \sum_{t=1}^T \|\epsilon_{\phi_i}(Emb_{T_i}, t, x_t) - \epsilon_0\|^2,$$

and the inner-loop update equation can be written as:

$$\phi_i = \phi_i - \eta \nabla L,$$

where  $t$  is the timestamp,  $\eta$  is the inner-loop learning rate,  $x_t = \sqrt{\bar{\alpha}_t} \mathbf{x}_0 + \sqrt{1 - \bar{\alpha}_t} \epsilon_0$ , and  $\bar{\alpha}_t = \prod_{j=1}^t \alpha_j$ . Note that  $L$  is the total loss of trajectory diffusion and the derivation of  $L$  is detailed in Section 3.1. According to REPTILE, the meta-update process can be written as:

$$\phi = \phi + \frac{\zeta}{n} \sum_{i=1}^n (\phi_i - \phi),$$

<sup>2</sup>This unusual index is set to match the index of diffusion algorithm in the following section.

<sup>3</sup>We will omit the diffusion model's condition state  $Emb_{T_i}$  in the following section for brevity.

---

### Algorithm 2 Lt-Di Training (whole-batch version)

---

**Require:** Initial model weights  $\phi$ , inner-loop steps  $K$ , learning rate  $\eta$ , meta-learning rate  $\zeta$ , and trajectory set  $\{Tra_1, \dots, Tra_n\}$ .

```

1: while not convergence do
2:   for  $i = 1, \dots, n$  do
3:      $\phi_i = \phi$ 
4:     for  $t = 1, \dots, K$  do
5:        $\phi_i = \phi_i - \eta \alpha \nabla_{\phi_i} L(\phi_i, Tra_i, t)$ 
6:     end for
7:      $\Delta_{\phi_i} = \phi_i - \phi$ 
8:   end for
9:    $\phi = \phi + \frac{\zeta}{n} \sum_{i=1}^n \Delta_{\phi_i}$ 
10: end while
    
```

---

where  $\zeta$  is the outer-loop learning rate and  $n$  is the total number of training tasks. The overall meta-learning process is shown in Algorithm 2.

## 2.3. Downstream Task Evaluation.

Based on the vanilla diffusion algorithm, the inference process of Lt-Di can be written as:

$$x_{t-1} = \frac{1}{\sqrt{\alpha_t}} x_t - \frac{1 - \alpha_t}{\sqrt{1 - \bar{\alpha}_t} \sqrt{\alpha_t}} \epsilon_\phi.$$

Through multiple inference processes, the well-trained denoiser  $\phi^*$  can recover the optimal head  $\theta^{h^*}$  from Gaussian-initialized weights.

## 3. Trajectory Diffusion and Analysis

In this section, we introduce the trajectory diffusion and analyze its configuration, principles, and convergence.

### 3.1. Trajectory Diffusion

Although we have established a general framework to meta-train the diffusion model, directly using it leads to sub-optimal performance. We denote the above method that combines meta-learning and vanilla diffusion as Lv-Di, i.e., Learning to Learn Weight Generation via Vanilla Diffusion. The right side of Figure 1 visualizes Lv-Di's inference chains in a 2D PAC-reduced weight landscape. In Omniglot's (Lake et al., 2011) 5-way 1-shot classification tasks, Lv-Di constrains only the inference endpoint, ignoring behavior along the inference chain. As a result, weights generated by Lv-Di will deviate from the ground truth (i.e., optimal weights). In Lt-Di, we use the whole optimization trajectory  $Tra = \{\theta_m^h, \dots, \theta_0^h\}$  rather than a single optimal weight  $\theta_0^h$  to guide the inference chain. According to the protocol given by DDPM,  $x_0$  equals  $\theta_0$ , and  $x_T$  is Gaussian noise that equals initial weights  $\theta_m^h$ . Thus, we can denote

the trajectory as  $Tra = \{\theta_m^h = x_{r(m)} = x_T, \dots, \theta_i^h = x_{r(i)}, \dots, \theta_0^h = x_0\}$ . Note that  $m < T$ , thus we need a function  $r(\cdot)$  that maps points in the optimization trajectory  $Tra$  to appropriate positions in the inference chain  $C_{infer} = \{x_T, \dots, x_0\}$ . We detail the selection of the mapping function  $r(\cdot)$  in Section 3.2.1. We derive the total loss  $L$  for trajectory diffusion as follows.

**Theorem 1.** *Given decay sequence  $\{\alpha_0, \dots, \alpha_T\}$ , and trajectory weight  $x_k$ . Let the inference equation align with the vanilla diffusion algorithm, i.e.,*

$$x_{t-1} = \frac{1}{\sqrt{\alpha_t}}x_t - \frac{1 - \alpha_t}{\sqrt{1 - \bar{\alpha}_t}\sqrt{\alpha_t}}\epsilon_\phi. \quad (1)$$

Then the diffusion model  $\epsilon_\phi$  can recover  $x_k$  from standard gaussian noise  $x_T$  in  $T - k$  steps, when  $\epsilon_\phi$  is trained by

$$L_k = \sum_{t=k+1}^T \|\sqrt{1 - \bar{\alpha}_t^k}\epsilon_\phi(x_t, t - k) - \sqrt{1 - \bar{\alpha}_t}\epsilon_k\|^2,$$

where  $x_t = \sqrt{\bar{\alpha}_t^k}\mathbf{x}_k + \sqrt{1 - \bar{\alpha}_t^k}\epsilon_k$ ,  $\bar{\alpha}_t = \prod_{j=1}^t \alpha_j$ ,  $\bar{\alpha}_t^k = \prod_{j=k+1}^t \alpha_j$ , and  $\epsilon_k$  denotes standard gaussian noise.

The proof is detailed in Appendix A. When  $k = 0$ , the loss given above is equivalent to the vanilla diffusion loss  $L_0$ , indicating that trajectory diffusion extends the original version. When  $L_0$  and  $L_k$  are optimized together, the denoising process enables the recovery of Gaussian noise  $x_T$  through two distinct pathways: a complete  $T$ -step process to reach  $x_0$ , and a partial  $T - k$  step process to reach  $x_k$ . Furthermore, due to the shared inference process defined in Equation 1, **the trajectory weight  $x_k$  appears within the  $T - k$  steps of  $x_0$ 's inference sequence.** As shown in the left side of Figure 1, compared to the vanilla diffusion model, additional trajectory weights can constrain the middle portion of the inference chain, thereby improving the generation quality of  $x_0$  at the end of the chain. Based on the above approach, **we can use each observed data point in trajectory  $Tra = \{x_{r(m)}, \dots, x_{r(i)}, \dots, x_{r(0)}\}$  to improve accuracy and efficiency.** The total trajectory loss  $L$  can be written as:

$$\begin{aligned} L &= \sum_{i=0}^m \gamma_i L_i \\ &= \sum_{i=0}^m \gamma_i \sum_{t=k+1}^T \|\sqrt{1 - \bar{\alpha}_t^k}\epsilon_\phi(x_t, t - k) - \sqrt{1 - \bar{\alpha}_t}\epsilon_k\|^2 \\ &\quad \cdot \mathbf{1}_{\{t \in (k, r(i+1)]\}} \end{aligned} \quad (2)$$

where  $k = r(i)$ ,  $x_t = \sqrt{\bar{\alpha}_t^k}\mathbf{x}_k + \sqrt{1 - \bar{\alpha}_t^k}\epsilon_k$ ,  $\bar{\alpha}_t = \prod_{j=1}^t \alpha_j$ ,  $\bar{\alpha}_t^k = \prod_{j=k+1}^t \alpha_j$ ,  $\gamma_i$  is the coefficient of  $L_i$ , and  $\epsilon_k$  is a standard Gaussian noise.

Theoretically, when  $t \in (k, r(i+1)]$ , we can use all  $x_0, \dots, x_k$  to guide this sub-inference chain. Nevertheless,

it leads to an overwhelming learning objective and more computational overhead. Therefore, we only use the nearest point  $x_k$  for learning, and that is why we need to multiply  $\mathbf{1}_{\{t \in (k, r(i+1)]\}}$  in  $L_i$ .

## 3.2. Analysis

In this section, we will discuss the configuration and principle issues raised in Section 2.1 and Section 3.1, and the convergence of the weight generation paradigm:

- How to configure trajectory diffusion?
- How does trajectory diffusion enable higher accuracy with efficient training and inference processes?
- The convergence properties of the weight generation paradigm and how to improve them.

### 3.2.1. TRAJECTORY DIFFUSION CONFIGURATION

First, we need to choose an index mapping function  $r(\cdot)$  that maps the trajectory weights in  $Tra_i = \{\theta_h^m, \dots, \theta_h^0\}$  to appropriate positions within the inference chain  $C_{infer} = \{x_T, \dots, x_0\}$ . In this paper, we map uniformly. Let the length of the optimization trajectory be  $m + 1$ , the length of the inference chain be  $T + 1$ , and assume that  $T + 1$  be divisible by  $m + 1$ , a trivial index mapping function  $r(\cdot)$  can be written as:

$$r(i) = \frac{i * T}{m} \quad (3)$$

Second, we need to determine the length of the optimization trajectory. This issue entails a trade-off between loss function complexity and accuracy gain from more trajectory weights. Under the constraint of three GPU hours, Figure 3 shows the relationship between the trajectory length and reconstruction MSE (Mean Square Error) between the predicted weight and the ground truth weight. We perform a case study on Omniglot (Lake et al., 2011) and Mini-Imagenet (Donahue et al., 2014) datasets for 5-way tasks. When the trajectory length is 2, it only includes  $x_T$  and  $x_0$ , which is equal to the vanilla diffusion model. As shown in Figure 3, although the best trajectory length may vary depending on task characteristics, all trajectory-based approaches outperform the vanilla version. These results suggest that trajectory diffusion can improve the generation quality. We set the default optimization trajectory length to 4, i.e.,  $m = 3$  in subsequent experiments.

### 3.2.2. TRAINING AND INFERENCE ACCELERATION

We can loosely reason by treating  $L$  as a linear combination of multiple optimization objectives. When  $m = 3$ , Figure 4 records three optimization objectives  $L_0, L_1$ , and  $L_2$ , corresponding to three trajectory weights,  $\theta_0, \theta_1$ , and

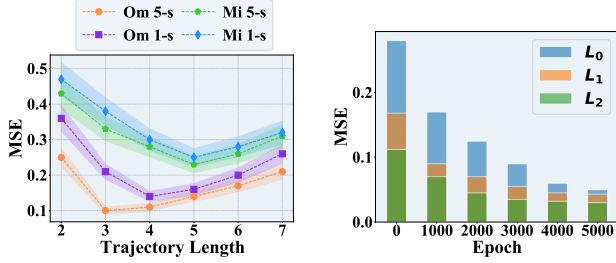


Figure 3. Trajectory length and MSE trade-off on 5-way tasks with 1-shot and 5-shot.

Figure 4. Convergence speed of each  $L_i$  on Omniglot 5-way 1-shot task.

$\theta_2$ , respectively. On Omniglot 5-way 1-shot tasks,  $L_2$  will converge first. This is because  $\theta_2$  is closest to Gaussian-initialized weight  $\theta_3$  and requires the fewest training epochs. Thus, the remaining learning target is to reconstruct  $\theta_0$  starting from  $\theta_2$ . By recursively applying this, a  $T$ -step diffusion problem breaks down into  $m$  shorter ones. Optimizing the original  $L_0$  is like finding a path within a hypersphere of radius  $T$ , while optimizing trajectory loss  $L$  is like working within  $m$  smaller hyperspheres of radius  $T/m$ . Obviously, the latter is easier to learn. As a result, with the same computational resources, the trajectory diffusion can achieve lower reconstruction error. Conversely, given the same target accuracy, the latter can tolerate fewer diffusion steps, thereby accelerating training and inference.

Figure 5 compares the trade-off curves between the vanilla diffusion and the trajectory diffusion on Omniglot and Mini-Imagenet 5-way 1-shot tasks. The left figure shows GPU-Hours vs. MSE trade-off and the right one is Diffusion Steps vs. MSE trade-off. As training progresses, the trajectory diffusion increasingly outperforms the vanilla version. The reason is that, in the early stages of training, trajectory diffusion primarily focuses on the learning of prerequisite objectives, such as  $L_2$ , rather than the ultimate target  $L_0$ . Once the learning of these prerequisite objectives is completed, trajectory diffusion converges faster to the optimal weights, i.e.,  $\theta_0$ . Benefiting from this, as shown in the right side of Figure 5, trajectory diffusion can tolerate fewer diffusion steps for the same MSE, thereby enhancing both training and inference efficiency.

### 3.2.3. CONVERGENCE ANALYSIS AND IMPROVEMENT

Learning to generate weights is an indirect approach compared to learning directly from downstream task samples, and its convergence can be challenging to guarantee. By assuming an upper bound on the generative model’s reconstruction error, the following analysis applies to all weight generation algorithms.

#### Assumption 1.

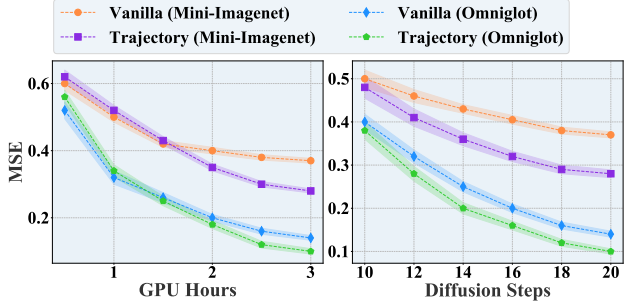


Figure 5. Comparison of trade-off curves between the vanilla diffusion and the trajectory diffusion on Mini-Imagenet and Omniglot 5-way 1-shot tasks. The left figure denotes GPU hours vs. MSE trade-off, and the right one denotes Diffusion Steps vs. MSE trade-off.

- 1. Reconstruction error upper bound.** The reconstruction error produced by the generative model is bounded by  $c$ .
- 2. Loss function upper bound.** The downstream task loss  $L_d(\cdot) \leq \psi$ .
- 3.  $l$ -smoothness.** There exists a constant  $l$  such that for all weights  $\theta, \theta' \in \mathbb{R}^n$

$$\|\nabla L_d(\theta) - \nabla L_d(\theta')\| \leq l\|\theta - \theta'\|$$

- 4.  $\mu$ -strong convexity.** There exists a constant  $\mu > 0$  such that for all  $\theta, \theta' \in \mathbb{R}^n$ ,

$$L_d(\theta') \geq L_d(\theta) + \nabla L_d(\theta)^\top (\theta' - \theta) + \frac{\mu}{2}\|\theta' - \theta\|^2.$$

- 5. Hessian matrix upper bound.** The Hessian matrix eigenvalue around the neighborhood of optimal weight  $\theta^*$  is bounded by  $\lambda$ .

**Theorem 2.** When Assumption 1 holds, Lt-Di’s cumulative empirical error can be bound by:

$$L_d(\hat{\theta}) - L_d(\theta^*) \leq \frac{\lambda}{2} \left[ c + \frac{2\psi}{\mu} \left( 1 - \frac{\mu}{l} \right)^{epoch} \right],$$

where  $epoch$  is the number of update steps used in the weight preparation stage, and  $\hat{\theta}$  is the weight predicted by the generative model.

The proof, provided in Appendix B, relies on the triangle inequality to decompose the accumulated error into weight preparation error and reconstruction error. We make a  $\mu$ -strong convex assumption here, but subsequent analysis and improvement do not rely on this property, thus preserving the practicality of our derivation. Theorem 2 shows that,

compared to direct learning methods, the reconstruction error of weight generation algorithms affects the upper bound of cumulative error in only a linear manner. Furthermore, this upper bound can be effectively improved by reducing the maximum eigenvalue  $\lambda$ . Penalizing the Hessian matrix is the simplest way to accelerate convergence, but it is computationally unacceptable.

In this paper, we penalize  $\lambda$  by constraining the curvature near the neighborhood of the optimal solution. We use Sharpness-Aware Minimization (SAM) (Foret et al., 2022) in the weight preparation stage to achieve the above target. As mentioned in Section 2.1, adding the additional SAM component doesn't incur additional time overhead. The process of SAM is shown in Algorithm 1.

### 4. Experiment

Our experimental platform includes two A100 GPUs, one Intel Xeon Gold 6348 processor, and 512 TB of DDR4 memory. For all experiment results, we report the mean and standard deviation over 5 independent repeated experiments. In the following section, we present the basic experimental results and setups, with more details provided in D.

#### 4.1. Ablation Study

##### 4.1.1. MAIN COMPONENTS

The advantages of Lt-Di stem from three main components:

- C1: Learning to generate optimal weights indirectly.
- C2: Using diffusion models to generate high-quality weights.
- C3: Using trajectory diffusion to guide the diffusion model.

As shown in Table 1, we validate the effectiveness of Lt-Di by ablating these components. When none of the components are used, Lt-Di degrades to the original REPTILE. When only C1 is used, we employ the vanilla VAE (Kingma & Welling, 2014) to generate weights, while we refer to this method as LLO-VAE. When using C1 and C2, Lt-Di degrades to Lv-Di. Results in Table 1 indicate that LLO-VAE demonstrates lower performance compared to REPTILE on the Omniglot dataset, suggesting the necessity for an enhanced generative algorithm. The comparison between REPTILE and Lv-Di shows that such an issue can be mitigated by using the diffusion model, which we attribute to its multi-step generation process that effectively captures the latent distribution of model weights. After adding the optimization trajectory, Lt-Di achieved the highest accuracy by modeling the entire optimization trajectory rather than just one optimal weight.

	C1	C2	C3	Omniglot	Mini-Imagenet
REPTILE				95.39 ± 0.35	47.07 ± 0.26
LLO-VAE	✓			94.92 ± 0.42	58.12 ± 0.28
Lv-Di	✓	✓		96.35 ± 0.21	66.90 ± 0.32
Lt-Di	✓	✓	✓	97.12 ± 0.23	68.10 ± 0.24

Table 1. Ablation main components on Omniglot and Mini-Imagenet datasets. Evaluate the accuracy of each variant on 5-way 1-shot tasks.

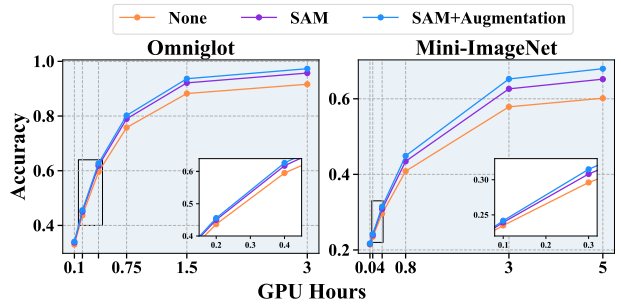


Figure 6. Ablation functional components on Omniglot and Mini-Imagenet datasets. Comparing Accuracy vs GPU Hours trade-off curve of each variant on 5-way 1-shot tasks.

##### 4.1.2. FUNCTIONAL COMPONENTS

Following the setup given by Finn et al. (2017), we conducted a case study to evaluate the accuracy improvement and overhead burden brought by each functional component. We incrementally added SAM and data augmentation components to Lt-Di's data preparation stage. In Omniglot and Mini-Imagenet datasets, we construct 5-way 1-shot tasks and record the model's accuracy on the meta-test set at each period of training. Figure 6 shows the GPU Hours vs. Accuracy trade-off curve in the meta-training stage. The results demonstrate that adding functional components can improve the model's performance without additional time overhead at any stage of training. As mentioned in 2.1, during meta-learning, the functional information is already included in the trajectory weights, allowing the meta-learning algorithm to focus solely on learning these weights. Therefore, the three models in the figure exhibit identical convergence rates and progressively increasing accuracy.

### 4.2. Comparison Experiments

#### 4.2.1. ZERO-SHOT TRANSFER LEARNING

**Task.** In this task, we train and evaluate models on disjoint pre-training and evaluation datasets. During evaluation, we do not use any labeled data to adjust the models. We evaluated the zero-shot transfer learning capability of the models using both accuracy and average per-sample evaluation la-

## Learning to Learn Weight Generation via Trajectory Diffusion

Learning Type	Method	CIFAR-10	CIFAR-100	STL-10	Aircraft	Pets	Latency (ms)
Directly Learning	REPTILE (Nichol et al., 2018)	48.31 ± 0.96	32.92 ± 0.61	45.25 ± 0.86	11.82 ± 2.84	17.25 ± 2.01	1.3
Directly Learning	Meta-Baseline (Chen et al., 2021b)	55.48 ± 0.64	40.52 ± 0.37	75.06 ± 0.17	19.17 ± 2.70	22.84 ± 1.25	1.4
Weights Generation	ICIS (Christensen et al., 2023)	61.75 ± 0.31	47.66 ± 0.24	80.59 ± 0.12	26.42 ± 1.56	28.71 ± 1.60	9.2
Weights Generation	GHN3 (Knyazev et al., 2023)	61.18 ± 0.28	49.94 ± 0.26	80.54 ± 0.14	26.46 ± 1.22	29.95 ± 1.75	14.5
Weights Generation	Lv-Di(ours)	61.74 ± 0.39	48.42 ± 0.26	78.89 ± 0.15	27.87 ± 1.67	29.53 ± 1.08	3.8
Weights Generation	Lt-Di(ours)	<b>62.07 ± 0.33</b>	<b>51.73 ± 0.25</b>	<b>81.64 ± 0.12</b>	<b>28.69 ± 1.14</b>	<b>31.88 ± 1.53</b>	2.6

Table 2. Zero-shot transfer learning accuracy comparison on various datasets with average per-sample evaluation latency.

Learning Type	Method	Omniglot				Mini-Imagenet				Latency (ms)
		(5, 1)	(5, 5)	(20, 1)	(20, 5)	(5, 1)	(5, 5)	(20, 1)	(20, 5)	
Direct Learning	REPTILE (Nichol et al., 2018)	95.39 ± 0.18	98.90 ± 0.14	88.14 ± 0.15	96.65 ± 0.33	47.07 ± 0.26	62.74 ± 0.37	38.24 ± 0.39	50.16 ± 0.46	20.7
Direct Learning	Meta-baseline (Chen et al., 2021b)	<b>97.75 ± 0.25</b>	<b>99.68 ± 0.18</b>	90.35 ± 0.20	96.92 ± 0.28	58.10 ± 0.31	74.50 ± 0.29	39.08 ± 0.40	52.14 ± 0.45	20.5
Weights Generation	Meta-Hypernetwork (Zhao et al., 2020)	96.57 ± 0.22	98.83 ± 0.16	89.90 ± 0.17	96.80 ± 0.30	60.51 ± 0.28	76.08 ± 0.34	40.07 ± 0.42	52.75 ± 0.48	13.1
Weights Generation	OCD (Lutati & Wolf, 2023)	95.04 ± 0.18	98.74 ± 0.14	89.25 ± 0.19	96.55 ± 0.25	62.76 ± 0.27	75.16 ± 0.35	41.53 ± 0.37	53.92 ± 0.46	8.4
Weights Generation	GHN3 (Knyazev et al., 2023)	95.23 ± 0.23	98.65 ± 0.19	89.07 ± 0.22	96.40 ± 0.31	66.22 ± 0.29	79.79 ± 0.33	44.10 ± 0.45	54.50 ± 0.50	22.5
Weights Generation	Meta-Diff (Zhang et al., 2024)	96.65 ± 0.20	98.91 ± 0.12	90.50 ± 0.16	97.11 ± 0.32	67.23 ± 0.33	80.81 ± 0.31	48.29 ± 0.39	59.25 ± 0.44	8.9
Weights Generation	Lv-Di(ours)	96.35 ± 0.21	98.83 ± 0.15	89.19 ± 0.18	96.70 ± 0.27	66.90 ± 0.32	80.25 ± 0.28	48.75 ± 0.38	59.95 ± 0.47	6.2
Weights Generation	Lt-Di(ours)	97.12 ± 0.23	99.42 ± 0.08	<b>90.83 ± 0.16</b>	<b>97.18 ± 0.25</b>	<b>68.10 ± 0.24</b>	<b>81.42 ± 0.30</b>	<b>51.29 ± 0.32</b>	<b>62.18 ± 0.45</b>	<b>4.3</b>

Table 3. Few-shot task accuracy comparison on Omniglot and Mini-Imagenet datasets with average per-sample evaluation latency.

tency.

**Dataset.** We partitioned ImageNet-1k (Deng et al., 2009) into 20k subsets of 50 classes each with 50 images per class per task for pre-training. The evaluation datasets are CIFAR-10, CIFAR-100 (Krizhevsky, 2009), STL-10 (Coates et al., 2011), Aircraft (Maji et al., 2013), and Pets (Parkhi et al., 2012).

**Baselines.** We benchmark against REPTILE (Nichol et al., 2018), Meta-Baseline (Chen et al., 2021b), ICIS (Christensen et al., 2023), and GHN3 (Knyazev et al., 2023). The first two directly learn from downstream task samples, while the others learn to generate weight. For all the aforementioned models, the downstream network uses ResNet12 (He et al., 2016) as body  $\theta^b$ , and a two-layer linear probe as head  $\theta^h$ . For denoiser  $\phi$ , we employ the same U-Net architecture given by (Ho et al., 2020) and maintain this setup across all experiments in this paper.

**Results.** Table 2 shows that Lt-Di consistently improves performance on all tasks while utilizing the same network architecture as other methods. Compared to the state-of-the-art method, Lt-Di improved accuracy by an average of 1.58% across five evaluation datasets. This result demonstrates the generalizability of Lt-Di, which can be well applied to zero-shot transfer learning scenarios. As mentioned in Section 4.1.2, Lt-Di also outperforms its simplified variants, i.e., REPTILE and Lv-Di, demonstrating that indirectly learning optimization trajectory improves the model’s generalization ability. In terms of overhead, except for directly learning algorithms, i.e., REPTILE and Meta-Baseline, which do not generate weights, Lt-Di exhibits the lowest evaluation latency among other methods, confirming its efficiency.

### 4.2.2. FEW-SHOT LEARNING

**Task.** Following the setup provided by Finn et al. (2017), we train and evaluate models on disjoint meta-training and

meta-testing tasks. During the evaluation stage, we use the support set in meta-test tasks to fine-tune the models, and then compare the accuracy and average per-sample evaluation latency on the query set.

**Dataset.** We use Omniglot (Lake et al., 2011) and Mini-Imagenet (Donahue et al., 2014) datasets for the construction of 5-way 1-shot, 5-way 5-shot, 20-way 1-shot, and 20-way 5-shot tasks. The classes of the meta-training and the meta-testing tasks are disjoint from each other.

**Baselines.** We benchmark against REPTILE (Nichol et al., 2018), Meta-baseline (Chen et al., 2021b), Meta-Hypernetwork (Zhao et al., 2020), OCD (Lutati & Wolf, 2023), GHN3 (Knyazev et al., 2023), and Meta-Diff (Zhang et al., 2024). Following the setting given by Finn et al. (2017), the downstream network uses four convolution blocks as body  $\theta^b$ , and a two-layer linear probe as head  $\theta^h$ .

**Results.** Table 2 shows that Lt-Di can improve performance on almost all tasks. Since the 5-way task of Omniglot is relatively easy to learn, the Meta-Baseline algorithm can achieve slightly higher accuracy in a direct learning manner. Compared to the latest methods, Lt-Di achieves an average accuracy increase of 1.10%. Compared to the current fastest weight generation algorithm, i.e., OCD, Lt-Di reduces evaluation latency by 48.81%. Note that the direct learning algorithms REPTILE and Meta-Baseline have the highest latency here, as they require gradient computation to complete fine-tuning.

### 4.2.3. MULTI-DOMAIN GENERALIZATION

**Task.** In this task, we explore the multi-domain generalizability of Lt-Di. We follow the few-shot task given by Guan et al. (2023) to evaluate the model’s performance.

**Dataset.** We use DomainNet (Leventidis et al., 2021) for the construction of 5-way 1-shot and 20-way 5-shot tasks.

## Learning to Learn Weight Generation via Trajectory Diffusion

Learning Type	Method	DomainNet		
		(5, 1)	(20, 5)	Latency(ms)
Direct Learning	REPTILE (Nichol et al., 2018)	48.13 ± 0.50	52.32 ± 0.42	26.8
Direct Learning	Meta-Baseline (Chen et al., 2021b)	50.54 ± 0.47	54.45 ± 0.40	26.2
Weights Generation	Meta-Hypernetwork (Zhao et al., 2020)	59.00 ± 0.39	63.32 ± 0.35	10.3
Weights Generation	OCD (Lutati & Wolf, 2023)	64.58 ± 0.42	67.10 ± 0.38	9.7
Weights Generation	GHN3 (Knyazev et al., 2023)	63.11 ± 0.36	66.42 ± 0.33	30.1
Weights Generation	Meta-Diff (Zhang et al., 2024)	64.24 ± 0.41	67.58 ± 0.39	10.9
Weights Generation	Lv-Di(ours)	66.75 ± 0.35	69.98 ± 0.32	7.0
Weights Generation	Lt-Di(ours)	<b>68.10 ± 0.33</b>	<b>72.42 ± 0.36</b>	5.2

Table 4. Multi-domain generalization accuracy comparison on DomainNet with 5-way 1-shot and 20-way 5-shot tasks.

Specifically, we use Clipart, Infograph, Painting, Quickdraw, and Real domains for meta-training, while Sketch domains for meta-testing. Under this setting, the tasks in the meta-training set may come from different domains, and the tasks in the meta-testing set may come from another unseen domain.

**Baselines.** We benchmark against REPTILE, Meta-baseline, Meta-Hypernetwork, GHN3, OCD, and Meta-Diff. The downstream network uses ResNet12 as body  $\theta^b$ , and a two-layer linear probe as head  $\theta^h$ .

**Results.** Table 4 shows that Lt-Di significantly outperforms current methods on few-shot multi-domain generalization tasks. Compared to the best-performing baseline Meta-Diff, Lt-Di achieved an average improvement of 4.35% in accuracy. It can be observed that, compared to direct learning methods REPTILE and Meta-Baseline, methods that indirectly learn the optimal weight exhibit a significant advantage gap. Building on these approaches, Lt-Di further learns the optimization trajectory, which enhances the model’s performance even more. In terms of overhead, Lt-Di reduces evaluation latency by 46.39% compared to OCD, showing the same advantage as in zero-shot and few-shot tasks.

### 4.2.4. LARGE LANGUAGE MODEL FINE-TUNING

**Task.** In this section, we demonstrate that Lt-Di can be applied to the fine-tuning of LLM by learning to generate LoRA (Hu et al., 2022) matrices for new tasks with low latency. We compared the algorithms in terms of their fine-tuning accuracy upon convergence and the latency required to achieve it.

**Datasets.** We conduct a case study to demonstrate the generalizability and efficiency of Lt-Di. We use five binary classification tasks, i.e., SST-2, QQP, RTE, WNIL, and CoLA from the GLUE (Wang et al., 2019) benchmark for pre-training. Then we use the other two tasks, i.e., MRPC and QNLI, to evaluate the performance of the methods.

**Baselines.** We benchmark against Full-fine-tuning baseline, LoRA (Hu et al., 2022), AdaLoRA (Zhang et al., 2023), DyLoRA (Zhuang et al., 2023), and FourierFT (Ma et al., 2023), which are all gradient-based fine-tuning algorithms. The large language model we fine-tuned is

fine-tuning Type	Method	MRPC		QNLI	
		Acc	Latency (h)	Acc	Latency (h)
Gradient-Based	Full-fine-tune	<b>90.24 ± 0.57</b>	1.47	92.84 ± 0.26	3.15
Gradient-Based	LoRA (Hu et al., 2022)	89.76 ± 0.69	0.81	<b>93.32 ± 0.20</b>	1.76
Gradient-Based	AdaLoRA (Zhang et al., 2023)	88.71 ± 0.73	0.74	93.17 ± 0.25	1.68
Gradient-Based	DyLoRA (Zhuang et al., 2023)	89.59 ± 0.81	0.76	92.21 ± 0.32	1.63
Gradient-Based	FourierFT (Ma et al., 2023)	90.03 ± 0.54	0.68	92.25 ± 0.15	1.55
Weights Generation	Lv-Di(ours)	88.15 ± 0.62	0.22	90.96 ± 0.18	0.48
Weights Generation	Lt-Di(ours)	89.03 ± 0.56	<b>0.19</b>	91.52 ± 0.22	<b>0.41</b>

Table 5. Accuracy and fine-tuning latency comparison on GLUE-MRPC and GLUE-QNLI tasks for different fine-tuning algorithms.

RoBERTa-base (Ma et al., 2023) and the LoRA matrices are generated following the fine-tuning process given by Ma et al. (2023). Note that Lt-Di is a meta-learning-based method that can learn on all training tasks, while other baselines are single-task fine-tuning methods that only work on one task. *Smart readers* may notice that Lt-Di requires extra time for meta-learning, but this approach is a one-time effort and shows better potential in multi-task fine-tuning scenarios.

**Results.** Table 5 shows that Lt-Di achieves comparable binary classification accuracy on two evaluation tasks compared to other gradient-based fine-tuning algorithms while significantly accelerating the fine-tuning speed by 300% to 400%. Through its implementation of meta-learning, Lt-Di demonstrates remarkable efficiency in capturing shared representations from pre-training tasks, enabling direct generation of task-specific LoRA matrices without the need for gradient computation.

## 5. Conclusion and Limitation

In this paper, we propose Lt-Di, which integrates the fast inference capability of weight generation and the cross-task transferability of bi-level optimization. Building on this, we further propose Trajectory Diffusion, enabling the model to capture the entire optimization trajectory, which enhances weight generation accuracy and efficiency. Finally, we theoretically and empirically demonstrate that the convergence of this indirect learning paradigm can be improved solely by constraining the eigenvalues of the Hessian matrix of the downstream tasks loss function, improving convergence efficiency without additional time overhead.

Our method is not well-suited for single-task learning scenarios, as such settings do not require frequent weight updates. In these cases, the benefits of Lt-Di in fine-tuning and inference do not sufficiently outweigh the computational overhead of training a diffusion model. For relatively simple tasks, such as the Omniglot 5-way 5-shot task in Section 4.2.2, our method does not provide further accuracy improvements. Moreover, further validation is needed on tasks beyond computer vision and natural language processing.

## Impact Statements

Theoretically, we extend the diffusion algorithm to Trajectory Diffusion and analyze the convergence of the weight generation paradigm. Practically, we validate our method across multiple multi-task scenarios.

## References

- Chen, J., Wu, X., Li, Y., Li, Q., Zhan, L., and Chung, F. A closer look at the training strategy for modern meta-learning. In Larochelle, H., Ranzato, M., Hadsell, R., Balcan, M., and Lin, H. (eds.), *Advances in Neural Information Processing Systems 33: Annual Conference on Neural Information Processing Systems 2020, NeurIPS 2020, December 6-12, 2020, virtual*, 2020.
- Chen, Q., Shui, C., and Marchand, M. Generalization bounds for meta-learning: An information-theoretic analysis. In Ranzato, M., Beygelzimer, A., Dauphin, Y. N., Liang, P., and Vaughan, J. W. (eds.), *Advances in Neural Information Processing Systems 34: Annual Conference on Neural Information Processing Systems 2021, NeurIPS 2021, December 6-14, 2021, virtual*, pp. 25878–25890, 2021a.
- Chen, Y., Liu, Z., Xu, H., Darrell, T., and Wang, X. Meta-baseline: Exploring simple meta-learning for few-shot learning. In *2021 IEEE/CVF International Conference on Computer Vision, ICCV 2021, Montreal, QC, Canada, October 10-17, 2021*, pp. 9042–9051. IEEE, 2021b.
- Christensen, A., Mancini, M., Koepke, A. S., Winther, O., and Akata, Z. Image-free classifier injection for zero-shot classification. In *IEEE/CVF International Conference on Computer Vision, ICCV 2023, Paris, France, October 1-6, 2023*, pp. 19026–19035. IEEE, 2023.
- Coates, A., Ng, A. Y., and Lee, H. An analysis of single-layer networks in unsupervised feature learning. In *Proceedings of the 14th International Conference on Artificial Intelligence and Statistics (AISTATS)*, pp. 215–223, 2011.
- Deng, J., Dong, W., Socher, R., Li, L.-J., Li, K., and Fei-Fei, L. Imagenet: A large-scale hierarchical image database. In *Proceedings of the IEEE Conference on Computer Vision and Pattern Recognition (CVPR)*, pp. 248–255. IEEE, 2009.
- Donahue, J., Jia, Y., Vinyals, O., Hoffman, J., Zhang, N., Tzeng, E., and Darrell, T. Decaf: A deep convolutional activation feature for generic visual recognition. In *Proceedings of the 31th International Conference on Machine Learning, ICML 2014, Beijing, China, 21-26 June 2014*, volume 32, pp. 647–655. JMLR.org, 2014.
- Fallah, A., Mokhtari, A., and Ozdaglar, A. E. On the convergence theory of gradient-based model-agnostic meta-learning algorithms. In Chiappa, S. and Calandra, R. (eds.), *The 23rd International Conference on Artificial Intelligence and Statistics, AISTATS 2020, 26-28 August 2020, Online [Palermo, Sicily, Italy]*, volume 108 of *Proceedings of Machine Learning Research*, pp. 1082–1092. PMLR, 2020.
- Finn, C., Abbeel, P., and Levine, S. Model-agnostic meta-learning for fast adaptation of deep networks. In *Proceedings of the 34th International Conference on Machine Learning, ICML 2017, Sydney, NSW, Australia, 6-11 August 2017*, volume 70, pp. 1126–1135. PMLR, 2017.
- Flennerhag, S., Schroecker, Y., Zahavy, T., van Hasselt, H., Silver, D., and Singh, S. Bootstrapped meta-learning. In *The Tenth International Conference on Learning Representations, ICLR 2022, Virtual Event, April 25-29, 2022*. OpenReview.net, 2022.
- Foret, P., Kleiner, A., Mobahi, H., and Neyshabur, B. Sharpness-aware minimization for efficiently improving generalization. In *Proceedings of the International Conference on Learning Representations (ICLR)*, 2022.
- Gozalo-Brizuela, R. and Garrido-Merchán, E. C. A survey of generative AI applications. *CoRR*, abs/2306.02781, 2023.
- Guan, J. and Lu, Z. Task relatedness-based generalization bounds for meta learning. In *The Tenth International Conference on Learning Representations, ICLR 2022, Virtual Event, April 25-29, 2022*. OpenReview.net, 2022.
- Guan, Y., Liu, Y., Zhou, K., and Huang, J. Hierarchical meta-learning with hyper-tasks for few-shot learning. In Frommholz, I., Hopfgartner, F., Lee, M., Oakes, M., Lalmas, M., Zhang, M., and Santos, R. L. T. (eds.), *Proceedings of the 32nd ACM International Conference on Information and Knowledge Management, CIKM 2023, Birmingham, United Kingdom, October 21-25, 2023*, pp. 587–596. ACM, 2023.
- Ha, D., Dai, A., and Le, Q. V. Hypernetworks. In *International Conference on Learning Representations (ICLR)*, 2017.
- He, K., Zhang, X., Ren, S., and Sun, J. Deep residual learning for image recognition. In *Proceedings of the IEEE Conference on Computer Vision and Pattern Recognition (CVPR)*, pp. 770–778. IEEE, 2016.
- Ho, J., Jain, A., and Abbeel, P. Denoising diffusion probabilistic models. In Larochelle, H., Ranzato, M., Hadsell, R., Balcan, M., and Lin, H. (eds.), *Advances in Neural Information Processing Systems 33: Annual Conference on Neural Information Processing Systems 2020, NeurIPS 2020, December 6-12, 2020, virtual*, 2020.
- Hospedales, T., Antoniou, A., Micaelli, P., and Storkey, A. Meta-learning in neural networks: A survey. *IEEE transactions on pattern analysis and machine intelligence*, 44(9):5149–5169, 2021.
- Hu, E. J., Shen, Y., Wallis, P., Allen-Zhu, Z., Li, Y., Wang, S., and Chen, W. LoRA: Low-rank adaptation of large language models. In *Proceedings of the International Conference on Learning Representations (ICLR)*, 2022.
- Jose, S. T. and Simeone, O. Information-theoretic generalization bounds for meta-learning and applications. *Entropy*, 23(1):126, 2021a.
- Jose, S. T. and Simeone, O. An information-theoretic analysis of the impact of task similarity on meta-learning. In *IEEE International Symposium on Information Theory, ISIT 2021, Melbourne, Australia, July 12-20, 2021*, pp. 1534–1539. IEEE, 2021b.
- Kingma, D. P. and Welling, M. Auto-encoding variational bayes. In *2nd International Conference on Learning Representations (ICLR)*, 2014. Presented at ICLR 2014 as a conference paper.

- Knyazev, B., Hwang, D., and Lacoste-Julien, S. Can we scale transformers to predict parameters of diverse imagenet models? In Krause, A., Brunskill, E., Cho, K., Engelhardt, B., Sabato, S., and Scarlett, J. (eds.), *International Conference on Machine Learning, ICML 2023, 23-29 July 2023, Honolulu, Hawaii, USA*, volume 202 of *Proceedings of Machine Learning Research*, pp. 17243–17259. PMLR, 2023.
- Krizhevsky, A. Learning multiple layers of features from tiny images. Technical report, University of Toronto, 2009.
- Lake, B. M., Salakhutdinov, R., Gross, J., and Tenenbaum, J. B. One shot learning of simple visual concepts. In *Proceedings of the 33th Annual Meeting of the Cognitive Science Society, CogSci 2011, Boston, Massachusetts, USA, July 20-23, 2011*. cognitivesciencesociety.org, 2011.
- Leventidis, A., Rocco, L. D., Gatterbauer, W., Miller, R. J., and Riedewald, M. Domainnet: Homograph detection for data lake disambiguation. In *Proceedings of the 24th International Conference on Extending Database Technology, EDBT 2021, Nicosia, Cyprus, March 23 - 26, 2021*, pp. 13–24. OpenProceedings.org, 2021.
- Luo, C. Understanding diffusion models: A unified perspective. *CoRR*, abs/2208.11970, 2022.
- Lutati, S. and Wolf, L. OCD: learning to overfit with conditional diffusion models. In Krause, A., Brunskill, E., Cho, K., Engelhardt, B., Sabato, S., and Scarlett, J. (eds.), *International Conference on Machine Learning, ICML 2023, 23-29 July 2023, Honolulu, Hawaii, USA*, volume 202 of *Proceedings of Machine Learning Research*, pp. 23157–23169. PMLR, 2023.
- Ma, S., Zhou, C., Xie, S., Chen, X., Liu, J., and Gao, J. Fourier frequency tuning for parameter-efficient fine-tuning. In *Proceedings of the IEEE/CVF Conference on Computer Vision and Pattern Recognition (CVPR)*, pp. 3456–3467, 2023.
- Maji, S., Rahtu, E., Kannala, J., Blaschko, M., and Vedaldi, A. Fine-grained visual classification of aircraft. In *arXiv preprint arXiv:1306.5151*, 2013.
- Nichol, A., Achiam, J., and Schulman, J. On first-order meta-learning algorithms. volume abs/1803.02999, 2018.
- Nirkin, Y., Wolf, L., and Hassner, T. Hyperseg: Patch-wise hyper-network for real-time semantic segmentation. In *IEEE Conference on Computer Vision and Pattern Recognition, CVPR 2021, virtual, June 19-25, 2021*, pp. 4061–4070. Computer Vision Foundation / IEEE, 2021.
- Parkhi, O. M., Vedaldi, A., Zisserman, A., and Jawahar, C. Cats and dogs. *IEEE Conference on Computer Vision and Pattern Recognition*, 2012.
- Raghu, A., Raghu, M., Bengio, S., and Vinyals, O. Rapid learning or feature reuse? towards understanding the effectiveness of MAML. In *8th International Conference on Learning Representations, ICLR 2020, Addis Ababa, Ethiopia, April 26-30, 2020*. OpenReview.net, 2020.
- Raghu, M., Gilmer, J., Yosinski, J., and Sohl-Dickstein, J. SVCCA: singular vector canonical correlation analysis for deep learning dynamics and interpretability. In Guyon, I., von Luxburg, U., Bengio, S., Wallach, H. M., Fergus, R., Vishwanathan, S. V. N., and Garnett, R. (eds.), *Advances in Neural Information Processing Systems 30: Annual Conference on Neural Information Processing Systems 2017, December 4-9, 2017, Long Beach, CA, USA*, pp. 6076–6085, 2017.
- Rombach, R., Blattmann, A., Lorenz, D., Esser, P., and Ommer, B. High-resolution image synthesis with latent diffusion models. In *IEEE/CVF Conference on Computer Vision and Pattern Recognition, CVPR 2022, New Orleans, LA, USA, June 18-24, 2022*, pp. 10674–10685. IEEE, 2022.
- Schürholt, K., Knyazev, B., Giró-i Nieto, X., and Borth, D. Hyper-representations as generative models: Sampling unseen neural network weights. In *Advances in Neural Information Processing Systems (NeurIPS)*, 2022.
- Wang, A., Singh, A., Michael, J., Hill, F., Levy, O., and Bowman, S. R. Glue: A multi-task benchmark and analysis platform for natural language understanding. *Proceedings of the International Conference on Learning Representations (ICLR)*, 2019.
- Zhang, B., Luo, C., Yu, D., Li, X., Lin, H., Ye, Y., and Zhang, B. Metadiff: Meta-learning with conditional diffusion for few-shot learning. In Wooldridge, M. J., Dy, J. G., and Natarajan, S. (eds.), *Thirty-Eighth AAAI Conference on Artificial Intelligence, AAAI 2024, Thirty-Sixth Conference on Innovative Applications of Artificial Intelligence, IAAI 2024, Fourteenth Symposium on Educational Advances in Artificial Intelligence, EAAI 2014, February 20-27, 2024, Vancouver, Canada*, pp. 16687–16695. AAAI Press, 2024.
- Zhang, R., Li, J., Xie, Y., Liu, X., Zhao, Y., Wang, Q., and Liu, Z. AdaLoRA: Towards efficient adaptive low-rank adaptation for large language models. In *Proceedings of the Conference on Neural Information Processing Systems (NeurIPS)*, pp. 5678–5689, 2023.
- Zhao, D., Kobayashi, S., Sacramento, J., and von Oswald, J. Meta-learning via hypernetworks. In *4th Workshop on Meta-Learning at NeurIPS 2020 (MetaLearn 2020)*. NeurIPS, 2020.
- Zhuang, X., Cheng, Y., Gan, Z., Liu, J., Liu, L., Chen, G., Zhang, H., Wang, M., Liu, S., and Gao, J. DyLoRA: Parameter-efficient tuning of pre-trained models via dynamic low-rank adaptation. In *Proceedings of the Association for Computational Linguistics (ACL)*, pp. 2345–2356, 2023.

## A. Theorem and Proof

Readers can refer to the derivation process of DDPM (Luo, 2022) to understand the following derivation.

**Theorem 1.** *Given decay sequence  $\{\alpha_0, \dots, \alpha_T\}$ , and trajectory weight  $x_k$ . Let the inference equation align with the vanilla diffusion algorithm, i.e.,*

$$x_{t-1} = \frac{1}{\sqrt{\alpha_t}} x_t - \frac{1 - \alpha_t}{\sqrt{1 - \bar{\alpha}_t} \sqrt{\alpha_t}} \epsilon_\phi. \quad (1)$$

Then the diffusion model  $\epsilon_\phi$  can recover the image  $x_k$  from standard Gaussian noise  $x_T$  in  $T - k$  steps, when  $\epsilon_\phi$  is trained by

$$L_k = \sum_{t=k+1}^T \|\sqrt{1 - \bar{\alpha}_t^k} \epsilon_\phi(x_t, t - k) - \sqrt{1 - \bar{\alpha}_t} \epsilon_k\|^2,$$

where  $x_t = \sqrt{\bar{\alpha}_t^k} \mathbf{x}_k + \sqrt{1 - \bar{\alpha}_t^k} \epsilon_k$ ,  $\bar{\alpha}_t = \prod_{j=1}^t \alpha_j$ ,  $\bar{\alpha}_t^k = \prod_{j=k+1}^t \alpha_j$ , and  $\epsilon_k$  denotes standard Gaussian noise.

*Proof.* Consider the diffusion chain  $C_{diff} = \{x_k, \dots, x_T\}$  and let sequence  $\{\alpha_{k+1}, \dots, \alpha_T\}$  be the corresponding decay schedule. According to vanilla diffusion model, to maximize the likelihood  $p(x_k)$  of observed data  $x_k$ , we need to minimize denoising matching term

$$\sum_{t=k+1}^T \mathbb{E}_{q(x_t|x_k)} [\text{D}_{\text{KL}}(q(x_{t-1}|x_t, x_k) \| p_\phi(x_{t-1}|x_t))]. \quad (2)$$

In the KL divergence bracket, the left term can be expended by the Bayesian Theorem. The right term is the inference process to be modeled with  $\phi$ , whose expectation is given by Equation 1. According to Bayes Theorem,

$$q(x_{t-1} | x_t, x_k) = \frac{q(x_t | x_{t-1}, x_k) q(x_{t-1} | x_k)}{q(x_t | x_k)}. \quad (3)$$

According to the Markov Rule and standard diffusion process,

$$q(x_t | x_{t-1}, x_k) = q(x_t | x_{t-1}) \sim \mathcal{N}(x_t; \sqrt{\alpha_t} x_{t-1} + \sqrt{1 - \alpha_t} \mathbf{I}). \quad (4)$$

Recursively using the diffusion process on  $\{x_k, \dots, x_{t-1}\}$ , we have

$$q(x_t | x_k) \sim \mathcal{N}(x_t; \sqrt{\bar{\alpha}_t^k} x_k, (1 - \bar{\alpha}_t^k) \mathbf{I}), \quad (5)$$

where  $\bar{\alpha}_t^k = \prod_{j=k+1}^t \alpha_j$ . Note that the coefficients here differ from those in the vanilla diffusion algorithm. According to Equation 5,  $q(x_{t-1}|x_k)$  can be written as

$$q(x_{t-1}|x_k) \sim \mathcal{N}(x_{t-1}; \sqrt{\bar{\alpha}_{t-1}^k} x_k, (1 - \bar{\alpha}_{t-1}^k) \mathbf{I}). \quad (6)$$

According to Equation 4 5 6, Equation 3 can be written as

$$\begin{aligned} q(x_{t-1} | x_t, x_k) &= \frac{q(x_t | x_{t-1}, x_k) q(x_{t-1} | x_k)}{q(x_t | x_k)} \\ &\sim \frac{\mathcal{N}(x_t; \sqrt{\alpha_t} x_{t-1}, (1 - \alpha_t) \mathbf{I}) \mathcal{N}(x_{t-1}; \sqrt{\bar{\alpha}_{t-1}^k} x_k, (1 - \bar{\alpha}_{t-1}^k) \mathbf{I})}{\mathcal{N}(x_t; \sqrt{\bar{\alpha}_t^k} x_k, (1 - \bar{\alpha}_t^k) \mathbf{I})} \\ &\propto \exp \left\{ -\frac{1}{2} \left( \frac{1}{(1 - \alpha_t)(1 - \bar{\alpha}_{t-1}^k)} \right) \left[ x_{t-1}^2 - 2 \frac{\sqrt{\alpha_t}(1 - \bar{\alpha}_{t-1}^k) x_t + \sqrt{\bar{\alpha}_{t-1}^k}(1 - \alpha_t) x_k}{1 - \bar{\alpha}_t^k} x_{t-1} \right] \right\}. \end{aligned}$$

According to the definition of Gaussian distribution, the variance of Equation 3 can be written as

$$\sigma_q(t) \propto \frac{(1 - \alpha_t)(1 - \bar{\alpha}_{t-1}^k)}{1 - \bar{\alpha}_t^k} \mathbf{I},$$

the expectation can be written as

$$\mu(x_t, x_k) \propto \frac{\sqrt{\alpha_t}(1 - \bar{\alpha}_{t-1}^k) x_t + \sqrt{\bar{\alpha}_{t-1}^k}(1 - \alpha_t) x_k}{1 - \bar{\alpha}_t^k}. \quad (7)$$

Recursively apply the reparameterization trick to Equation 4 in an iterative manner, we have

$$x_t = \sqrt{\bar{\alpha}_t^k} x_k + \sqrt{1 - \bar{\alpha}_t^k} \epsilon_k. \quad (8)$$

This step is relatively complex, it is recommended to refer to Luo (2022). Reorganize Equation 8, we have

$$x_k = \frac{1}{\sqrt{\bar{\alpha}_t^k}} (x_t - \sqrt{1 - \bar{\alpha}_t^k} \epsilon_k).$$

Substitute  $x_k$  into Equation 7, we have

$$\begin{aligned} \mu(x_t, x_k) &\propto \frac{\sqrt{\alpha_t}(1 - \bar{\alpha}_{t-1}^k) x_t + \sqrt{\bar{\alpha}_{t-1}^k}(1 - \alpha_t) \frac{1}{\sqrt{\bar{\alpha}_t^k}} (x_t - \sqrt{1 - \bar{\alpha}_t^k} \epsilon_k)}{1 - \bar{\alpha}_t^k} \\ &= \frac{1}{\sqrt{\alpha_t}} x_t - \frac{1 - \alpha_t}{\sqrt{1 - \bar{\alpha}_t^k} \sqrt{\alpha_t}} \epsilon_k. \quad (9) \end{aligned}$$

Returning to Equation 2, minimizing KL divergence is equivalent to minimizing the difference between the expectations of the two terms in the bracket. Equation 1 gives the expectation of the right term, i.e.,

$$x_{t-1} = \frac{1}{\sqrt{\alpha_t}} x_t - \frac{1 - \alpha_t}{\sqrt{1 - \bar{\alpha}_t} \sqrt{\alpha_t}} \epsilon_\phi.$$

Equation 9 is the expectation of the left term. As a result, Equation 2 can be optimized by loss function

$$\begin{aligned} L_k &= \sum_{t=k+1}^T \|\mu(x_t, x_k) - \mu_\phi(x_t, t)\|^2 \\ &= \sum_{t=k+1}^T \frac{(1 - \alpha_t)^2}{\alpha_t(1 - \bar{\alpha}_t^k)(1 - \bar{\alpha}_t)} \|\sqrt{1 - \bar{\alpha}_t^k} \epsilon_\phi(x_t, t - k) - \sqrt{1 - \bar{\alpha}_t} \epsilon_k\|^2 \\ &\propto \sum_{t=k+1}^T \|\sqrt{1 - \bar{\alpha}_t^k} \epsilon_\phi - \sqrt{1 - \bar{\alpha}_t} \epsilon_k\|^2. \end{aligned}$$

Since the only observed data is  $x_k$ , and to satisfy total  $T - k$  steps,  $\epsilon_\phi$  can be written as

$$\epsilon_\phi := \epsilon_\phi(\sqrt{\bar{\alpha}_t^k} \mathbf{x}_k + \sqrt{1 - \bar{\alpha}_t^k} \epsilon_k, t - k). \quad \square$$

## B. Theorem and Proof

### Assumption 1.

1. **Reconstruction error upper bound.** The reconstruction error produced by the generative model is bounded by  $c$ .

2. **Loss function upper bound.** Downstream task loss  $L_d(\cdot) \leq \psi$ .

3.  **$l$ -smoothness.** There exists a constant  $l$  such that for all weights  $\theta, \theta' \in \mathbb{R}^n$

$$\|\nabla L_d(\theta) - \nabla L_d(\theta')\| \leq l\|\theta - \theta'\|$$

4.  **$\mu$ -strong convex.** There exists a constant  $\mu > 0$  such that for all  $\theta, \theta' \in \mathbb{R}^n$ ,

$$L_d(\theta') \geq L_d(\theta) + \nabla L_d(\theta)^\top (\theta' - \theta) + \frac{\mu}{2}\|\theta' - \theta\|^2.$$

5. **Hessian matrix upper bound.** The Hessian matrix eigenvalue around the neighborhood of optimal weight  $\theta^*$  is bounded by  $\lambda$ .

**Lemma 1.** Assume that the loss function  $L_d(\cdot)$  is  $l$ -smooth and satisfies  $\mu$ -strongly convex. Then, the sequence  $\{\theta_i\}_{i=0}^{epoch}$  generated by the gradient descent update with step size  $\frac{1}{l}$  satisfies

$$\|\theta^{epoch} - \theta^*\|^2 \leq \frac{2[L_d(\theta^0) - L_d(\theta^*)]}{\mu} \left(1 - \frac{\mu}{l}\right)^{epoch}.$$

*Proof.* Since  $L_d(\theta)$  is  $l$ -smooth, for any  $\theta$  and  $\theta'$ ,

$$L_d(\theta') \leq L_d(\theta) + \nabla L_d(\theta)^\top (\theta' - \theta) + \frac{l}{2}\|\theta' - \theta\|^2.$$

Applying this to the gradient descent update  $\theta^{k+1} = \theta^k - \frac{1}{l}\nabla L_d(\theta^k)$ , we have

$$\begin{aligned} L_d(\theta^{k+1}) &\leq L_d(\theta^k) + \nabla L_d(\theta^k)^\top (\theta^{k+1} - \theta^k) + \frac{l}{2}\|\theta^{k+1} - \theta^k\|^2 \\ &= L_d(\theta^k) - \frac{1}{2l}\|\nabla L_d(\theta^k)\|^2. \end{aligned} \quad (10)$$

Since  $L_d(\theta)$  is  $\mu$ -strongly convex, it satisfies the Polyak-Lojasiewicz condition:

$$\frac{1}{2}\|\nabla L_d(\theta)\|^2 \geq \mu[L_d(\theta) - L_d(\theta^*)].$$

Substituting this inequality into Equation 10, we have

$$L_d(\theta^{k+1}) \leq L_d(\theta^k) - \frac{\mu}{l}(L_d(\theta^k) - L_d(\theta^*)).$$

The above equation can be reorganized to

$$L_d(\theta^{k+1}) - L_d(\theta^*) \leq \left(1 - \frac{\mu}{l}\right)(L_d(\theta^k) - L_d(\theta^*)).$$

Start from  $k = 0$ , and recursively apply the above equation with  $epoch$  times. It follows that

$$L_d(\theta^{epoch}) - L_d(\theta^*) \leq \left(1 - \frac{\mu}{l}\right)^{epoch} (L_d(\theta^0) - L_d(\theta^*)).$$

Since  $L_d(\theta)$  is  $\mu$ -strongly convex, it satisfies

$$\|\theta - \theta^*\|^2 \leq \frac{2}{\mu}(L_d(\theta) - L_d(\theta^*)).$$

So we have

$$\begin{aligned} \|\theta^{epoch} - \theta^*\|^2 &\leq \frac{2}{\mu}(L_d(\theta^{epoch}) - L_d(\theta^*)) \\ &\leq \frac{2(L_d(\theta^0) - L_d(\theta^*))}{\mu} \left(1 - \frac{\mu}{l}\right)^{epoch}. \end{aligned}$$

□

**Theorem 2.** When Assumption 1 holds, Lt-Di's cumulative empirical error can be bound by:

$$L_d(\hat{\theta}) - L_d(\theta^*) \leq \frac{\lambda}{2} \left[ c + \frac{2\psi}{\mu} \left(1 - \frac{\mu}{l}\right)^{epoch} \right],$$

where  $epoch$  is the number of update steps used in the weight preparation stage, and  $\hat{\theta}$  is the weight predicted by the generative model.

*Proof.* Using the Taylor expansion around the optimal point  $\theta^*$ , we have

$$\begin{aligned} L_d(\hat{\theta}) - L_d(\theta^*) &= \nabla L_d(\theta^*)^\top (\hat{\theta} - \theta^*) + \frac{1}{2}(\hat{\theta} - \theta^*)^\top \nabla^2 L_d(\xi) (\hat{\theta} - \theta^*) \\ &= \frac{1}{2}(\hat{\theta} - \theta^*)^\top \nabla^2 L_d(\xi) (\hat{\theta} - \theta^*). \end{aligned} \quad (11)$$

According to a constraint on the Hessian matrix, we have

$$\frac{1}{2}(\hat{\theta} - \theta^*)^\top \nabla^2 L_d(\xi) (\hat{\theta} - \theta^*) \leq \frac{\lambda}{2}\|\hat{\theta} - \theta^*\|^2. \quad (12)$$

Decomposing  $|\hat{\theta} - \theta^*|^2$  into weight preparation error and reconstruction error, we have

$$\begin{aligned} \|\hat{\theta} - \theta^*\|^2 &\leq \|\hat{\theta} - \theta^{epoch}\|^2 + \|\theta^{epoch} - \theta^*\|^2 \\ &\leq c + \frac{2(L_d(\theta^0) - L_d(\theta^*))}{\mu} \left(1 - \frac{\mu}{l}\right)^{epoch} \\ &\leq c + \frac{2\psi}{\mu} \left(1 - \frac{\mu}{l}\right)^{epoch}. \end{aligned} \quad (13)$$

Substituting Equation 13 and Equation 12 into Equation 11 we obtain

$$L_d(\hat{\theta}) - L_d(\theta^*) \leq \frac{\lambda}{2} \left[ c + \frac{2\psi}{\mu} \left(1 - \frac{\mu}{l}\right)^k \right].$$

□

## C. Preliminary

### C.1. Symbol Table

Potentially ambiguous symbols are described in Table 6 to enhance the reader’s comprehension of this paper.

Symbol	Description
$\epsilon$	Gaussian noise.
$\phi$	Diffusion model, i.e., denoiser.
$\{\alpha_i\}_{i=0}^T$	Decay schedule for diffusion process.
$C_{infer}$	Inference chain of the diffusion model.
$Tra$	Optimization trajectory.
$r(\cdot)$	Function that maps $Tra$ to $C_{infer}$
$x_i$	Element of the inference chain.
$\theta^b$	Body, i.e., bottleneck of the downstream network, also used for task embedding.
$\theta^h$	Head of the downstream network.
$\hat{\theta}$	Weight generated by the diffusion model.
$\eta$	Inner-loop learning rate.
$\zeta$	Outer-loop learning rate.
$K$	Number of Inner-loop step.

Table 6. Symbols and their descriptions.

### C.2. Diffusion Model

The core idea of the diffusion model is to model data through a two-stage process:

- **Diffusion Process:** Starting with data  $x_0$ , noise is added at each step to generate  $x_T$ , eventually approaching a standard normal distribution.
- **Inference Process:** Starting with noise  $x_T$ , a denoising model  $\phi$  generates  $x_{T-1}, x_{T-2}, \dots, x_0$  step by step.

By precisely modeling the reverse process, the diffusion model  $\phi$  can generate new samples that match the original data distribution. Diffusion models define a decay schedule  $\{\alpha_i\}_{i=0}^T$  to control the noise level at each step. In the diffusion process, noise is added at each step  $t$ , transforming the data  $x_{t-1}$  into  $x_t$

$$q(x_t|x_{t-1}) = \mathcal{N}(x_t; \sqrt{\alpha_t}x_{t-1}, (1 - \alpha_t)\mathbf{I}).$$

The direct transition from  $x_0$  to  $x_t$  can be written as

$$q(x_t|x_0) = \mathcal{N}(x_t; \sqrt{\bar{\alpha}_t}x_0, (1 - \bar{\alpha}_t)\mathbf{I}),$$

where  $\bar{\alpha}_t = \prod_{i=1}^t \alpha_i$  is the cumulative noise schedule, controlling the overall noise level from  $x_0$  to  $x_t$ . In the inference process, the denoiser iteratively reconstructs the data by

$$x_{t-1} = \frac{1}{\sqrt{\alpha_t}}x_t - \frac{1 - \alpha_t}{\sqrt{1 - \bar{\alpha}_t}\sqrt{\alpha_t}}\epsilon_\phi + \sigma_z\epsilon,$$

We omit additional  $\sigma_z\epsilon$  for stable weight generation. The key point of training a variational model is to maximize the Evidence Lower Bound(ELBO). In the diffusion algorithm, optimizing the ELBO is essentially equivalent to minimizing the denoising match term

$$\sum_{t=k+2}^T \mathbb{E}_{q(x_t|x_k)} [\text{D}_{\text{KL}}(q(x_{t-1}|x_t, x_k) \| p_\phi(x_{t-1}|x_t))],$$

which is also the objective optimized by our trajectory diffusion.

### C.3. REPTILE

REPTILE is a first-order optimization-based meta-learning algorithm that simplifies training while retaining strong adaptability across tasks. It eliminates the need for second-order gradients, making it computationally efficient compared to algorithms like MAML. The training process consists of two loops: the inner-loop and the outer-loop.

In the inner loop, REPTILE performs gradient descent on a sampled task  $T_i$  using the task’s support set. Starting from the meta-parameters  $\theta$ , the task-specific parameters  $\theta_i$  are updated for  $K$  steps using

$$\theta_i^{(t+1)} = \theta_i^{(t)} - \eta \nabla_{\theta_i^{(t)}} L_{T_i}(\theta_i^{(t)}),$$

where  $\eta$  is the inner-loop learning rate and  $L_{T_i}$  is the loss for task  $T_i$ .

In the outer-loop, the meta-parameters  $\theta$  are updated by moving them toward the task-specific parameters  $\theta_i$  obtained from the inner loop. This meta-update is given by

$$\theta \leftarrow \theta + \zeta(\theta_i - \theta),$$

where  $\zeta$  is the outer-loop learning rate.

By iteratively repeating the inner and outer loops across multiple tasks drawn from the task distribution  $p(T)$ , REPTILE optimizes the meta-parameters  $\theta$  to find an initialization that enables fast adaptation to new tasks with minimal gradient steps. Its simplicity lies in avoiding second-order derivatives, while its effectiveness is demonstrated across diverse applications such as few-shot learning and domain generalization.

## D. Experimental Detail

### D.1. Dataset

**Omniglot.** The raw Omniglot dataset contains 1623 handwritten characters from 50 alphabets, each with 20 instances in  $28 \times 28$  grayscale format. We partition the classes of training set, evaluation set, and testing set into 800:400:432. We use Omniglot in three scenarios. We used the Omniglot dataset in our preliminary experiments, ablation experiments, and comparative experiments. For the construction of the classification task, we referred to the experimental setup by Chelsea Finn et al.(MAML).

**Mini-Imagenet.** The raw Mini-Imagenet contains 100 classes, each containing 600 instances in  $84 \times 84$  grayscale format. We partition classes of training set, evaluation set, and testing set into 64:16:20. The usage of Mini-Imagenet is the same as Omniglot, and we also follow the setup given by Chelsea Finn et al.

**Imagenet-1K.** The raw ImageNet-1K is a benchmark dataset with 1000 classes, 1.2 million training images, and 50000 validation images, typically resized to a resolution of  $224 \times 224$  pixels. We partitioned the dataset into 20k subsets, each containing 50 classes with 50 images per class. We use this dataset for pre-training and perform transfer zero-shot evaluation on other unseen datasets.

**CIFAR-10 CIFAR-100 STL-10 Aircraft Pets.** CIFAR-10 and CIFAR-100 are image datasets introduced by Alex Krizhevsky, containing 60000 images resized to  $32 \times 32$  pixels. CIFAR-10 includes 10 classes, while CIFAR-100 features 100 fine-grained classes. STL-10, derived from ImageNet, consists of 10 classes with 13000 labeled images and 100000 unlabeled images, with a resolution of  $96 \times 96$  pixels. The Aircraft dataset includes 10000 images across 100 aircraft models, with hierarchical labels for manufacturer, family, and variant. The Pets dataset consists of 7349 images of 37 pet breeds, with annotations for class labels, bounding boxes, and pixel-level segmentation. We use these datasets to evaluate the model’s transfer zero-shot learning capabilities, which means the labels of these datasets are not visible to the model.

**DomainNet.** DomainNet is a dataset for multi-domain generalization. We use it to evaluate algorithms’ ability of few-shot domain generalization. It consists of 345 classes from 6 domains, with a resolution of  $224 \times 224$  pixels. We use Clipart, Infograph, Painting, Quickdraw, and Real domains for training, while Sketch domains for testing. The tasks we constructed are 5-way 1-shot and 20-way 5-shot. Note that the testing set shares the same 345 classes as the

training set.

**GLUE.** The GLUE Benchmark (General Language Understanding Evaluation) tests models on 9 diverse NLP tasks, including CoLA for grammatical acceptability, SST-2 for sentiment classification, MRPC for paraphrase detection, STS-B for sentence similarity, QQP for duplicate question detection, MNLI for natural language inference, QNLI for question-answer validation, RTE for entailment classification, and WNLI for pronoun resolution. We use this dataset to test the efficiency of different algorithms for multi-task fine-tuning on LLM models. Specifically, we use five binary classification tasks, i.e., SST-2, QQP, RTE, WNLI, and CoLA for the training of LLWTD. Then we use the other two tasks, i.e., MRPC and QNIL, to evaluate the performance of different fine-tuning algorithms.

Note that all hyperparameters are obtained on Omniglot and Mini-Imagenet datasets, so other datasets don’t need a validation set.

### D.2. Model Configuration

Lt-Di involves hyperparameter configurations in two components: downstream network  $\theta$  and diffusion model  $\phi$ . For the downstream network  $\theta$ , we adopt different architectures for different tasks. In tasks on the Omniglot and Mini-ImageNet datasets, we follow the standard setup used by most meta-learning methods, employing 4 convolution blocks with batch normalization and ReLU as the body  $\theta^b$  and 2 fully connected layers as the head  $\theta^h$ . For zero-shot tasks on CIFAR-10, CIFAR-100, STL-10, Aircraft, and Pets, we use the commonly adopted ResNet-12 as the body and still employ a 2-layer fully connected head. In multi-domain generalization tasks, we maintain the same setup. In the LLM multi-task fine-tuning scenario, the downstream network is the LLM model itself, i.e., RoBERTa-base with 125 million weights. For the diffusion model  $\phi$ , we use the commonly adopted U-Net architecture. The number of inference steps in the diffusion model is set to 20, as shown in Figure 5. The length of the selected optimization trajectory is set to 4, as indicated in Figure 3. For LLWD, it maintains the same setup as LLWTD, with the difference that the length of the optimization trajectory is set to 2. Finally, for the meta-learning algorithm, we use REPTILE, a first-order gradient algorithm that does not differentiate between the support set and the query set. The inner-loop learning rate is set to 0.05, the outer-loop learning rate to 0.001, and the optimizer for both is Adam.

### D.3. Sensitive Study

Compared to existing weight generation methods, the two hyperparameters of Lt-Di, i.e., trajectory length and diffu-

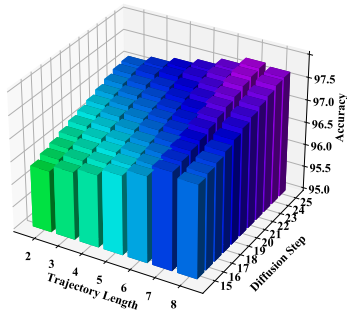


Figure 7. Sensitive study on Omniglot

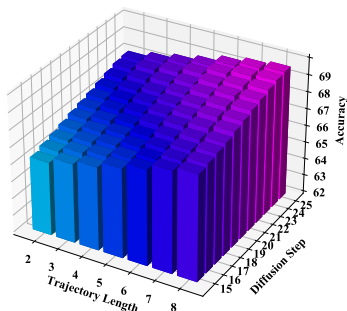


Figure 8. Sensitive study on Mini-Imagenet

sion steps, may affect the model’s sensitivity. To evaluate the robustness of our approach, we analyze the impact of trajectory length and diffusion steps on classification accuracy for Mini-ImageNet and Omniglot. As shown in Figure 7 and Figure 8, the accuracy remains stable across different parameter settings, with only minor variations. While increasing trajectory length and diffusion steps can slightly improve performance, excessive changes do not lead to significant degradation. The consistency across both datasets indicates that Lt-Di is insensitive to these hyperparameters, demonstrating robustness. Note that we do not use the parameter combination that achieves the highest accuracy in this experiment as the default setting. We aim to maintain performance above current state-of-the-art levels while reducing computational costs during inference.

#### D.4. Adaptability to Different Architectures

To verify the effectiveness of Lt-Di under network structures of different scales, we compare it with its degraded versions, i.e., REPTILE, LLO-VAE, and Lv-Di. Table 7 and Table 8 show the effectiveness of our method on Swin Transformer, ResNet18, and MobileNetV2 architectures. The results demonstrate that each component of our method remains effective across neural network architectures of different scales.

Method	Swin Transformer	ResNet18	MobileNetV2
REPTILE	98.27	97.11	93.79
LLO-VAE	97.43	96.60	93.61
Lv-Di	98.93	98.44	94.92
Lt-Di	99.90	98.82	95.84

Table 7. Comparison of Accuracy across different network structures on Omniglot 5-way 1-shot tasks.

Method	Swin Transformer	ResNet18	MobileNetV2
REPTILE	57.27	52.55	40.67
LLO-VAE	66.26	60.32	53.27
Lv-Di	76.75	70.76	59.33
Lt-Di	82.38	77.85	64.81

Table 8. Comparison of Accuracy across different network structures on Mini-Imagenet 5-way 1-shot tasks.

## E. Related Work

**Meta-Learning.** Meta-learning often employs a bi-level optimization-based paradigm (Finn et al., 2017; Raghu et al., 2020; Chen et al., 2021b; Flennerhag et al., 2022; Fallah et al., 2020) for better generalization performance (Jose & Simeone, 2021a;b; Chen et al., 2021a; Guan & Lu, 2022; Chen et al., 2020) on few-shot and reinforcement learning tasks. However, it incurs significant costs for weight fine-tuning, especially in multi-task scenarios. Methods like ANIL (Raghu et al., 2020) and Reptile (Nichol et al., 2018) improve training efficiency by minimizing updates to only essential task-specific layers or by approximating meta-gradients, respectively. However, these methods still rely on gradient computation and fail to achieve superior accuracy.

**Network Weights Generation.** Hypernetwork (Ha et al., 2017) is the first method that uses one network to generate another’s weights, leading to extensions like the HyperSeg (Nirkin et al., 2021) for downstream task flexibility. Conditional diffusion models provide another approach, with OCD leveraging overfitting (Lutati & Wolf, 2023) and Meta-Diff enhancing few-shot adaptability (Zhang et al., 2024). Hyper-representations (Schürholt et al., 2022) embed model characteristics to support weight generation for unseen tasks, while Image-free Classifier Injection (Christensen et al., 2023) achieves zero-shot classification via semantic-driven weights. These methods are constrained by their single-level optimization approach, which presents limitations in both cross-task knowledge transfer capabilities and potential adaptability to novel tasks. Most importantly, these methods overlook the role of other weights, limiting the model’s efficiency and accuracy.